2008

NANOMAGNETICS INSTRUMENTS

[HALL PROBE GRADIOMETRY]

A novel Scanning Hall probe gradiometer has been developed and a new method to image x, y & z components of the magnetic field on the sample surface has been demonstrated for the first time with 1µm spatial resolution. 3D field distribution of a Hard Disk sample is successfully measured at 77K using this novel approach to prove the concept.

1.1 Novel Hall Probe Gradiometry

The gradiometry in the general sense describes the method used to measure the variation of a physical quantity in space. In our case it is the magnetic field variation over the sample. From Figure 1 it can be seen that if a different voltage value is measured through terminals $V_{1\text{-}2}$ and $V_{3\text{-}4}$ due to the presence of an external magnetic field up on the Hall array, this indicates a field variation along the current axis. The magnitude of the voltage difference can be used to quantify this variation. This is a one dimensional first order gradiometer configuration. Number of terminals can be increased but the separation between them should be as much as the width of the Hall crosses.

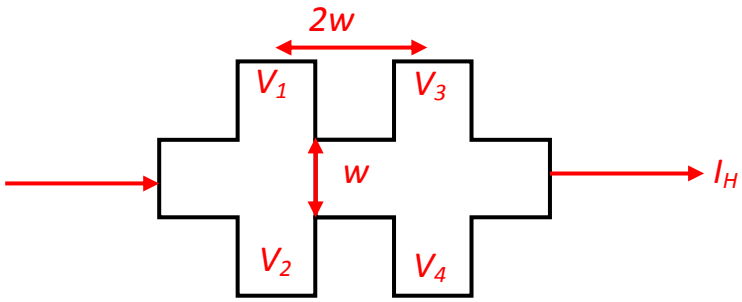

Figure 1: Hall gradiometer.

The method used in this study, however, is completely different than the methods described above. There is no need for the complex design principles or the growth requirements. Any semiconducting material suitable for a Hall effect device is applicable with a simple fabrication process. The spatial resolution is just defined by the width of the Hall cross, thus the limitation only comes from the fabrication capability or from the material properties, such as the surface charge depletion after certain size. In fact, probes with ~50nm spatial resolution has already been shown [1], which can readily be employed to measure the three dimensional magnetic fields using that method.

The low noise amplifier is modified such that, the current and voltage signals can be passed through any four leads of the Hall cross. The restriction of having the current and the voltage leads to be mutually perpendicular to each other is eliminated. If the current flow does not follow a straight path as shown in Fig. 2, we still observe the Hall effect, which we may call the bending resistance [2-3]. As the current flows at any particular point along the path, the magnetic force F_M is perpendicular to the direction of motion. In uniform magnetic field however, the Hall voltage would be equal to zero. But, if the magnetic field distribution across the device is spatially non-uniform and nonsymmetrical along the gradient axis, there will be a finite voltage developed at the voltage terminals. The lateral electric field $\vec{E}$ generated to balance the magnetic force is not uniform across the device; in other words, it has a gradient along the device. As a result, the measured potential is the derivative of the perpendicular magnetic field in the active region of the Hall cross. Depending on the current flow path the derivative about to different diagonals of the Hall cross is measured as shown in Fig. 3 with the non-perpendicular current and voltage leads with different configurations and the field gradient axis. This has been accidentally observed by Bath University group [4] during an SHPM experiment, where the voltage and current leads were mixed up. The orientation of the sensor over the magnetic field distribution of the measured sample is important. In our setup the probe has a fixed position with respect to the quadrants of the scanner piezo. Thus, the orientation of the probe is not changing during the scan which is placed by 45º with respect to the X&Y scan directions (Fig.4). On the other hand the sample can be aligned in any desired rotational angle with respect to our Hall sensor. In the experiments a hard disk sample is imaged with a 1μm size PHEMT Hall probe in LN_2 environment to minimize the thermal drift. First, an image is obtained using the normal Hall sensor configuration, where current and voltage leads were perpendicular to each other.

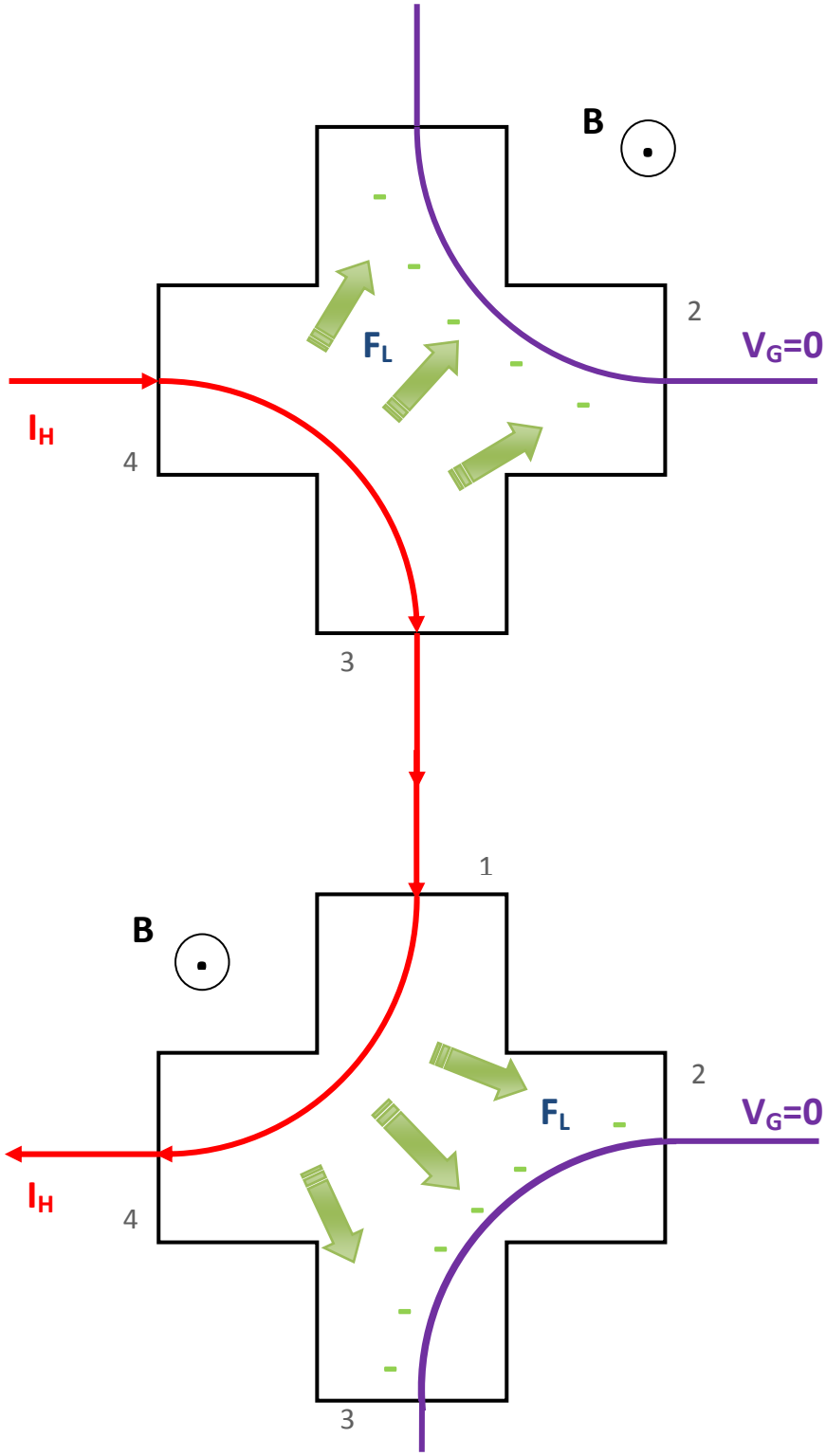

Figure 2: Hall effect with non-perpendicular current and voltage leads with different configurations under uniform magnetic field.

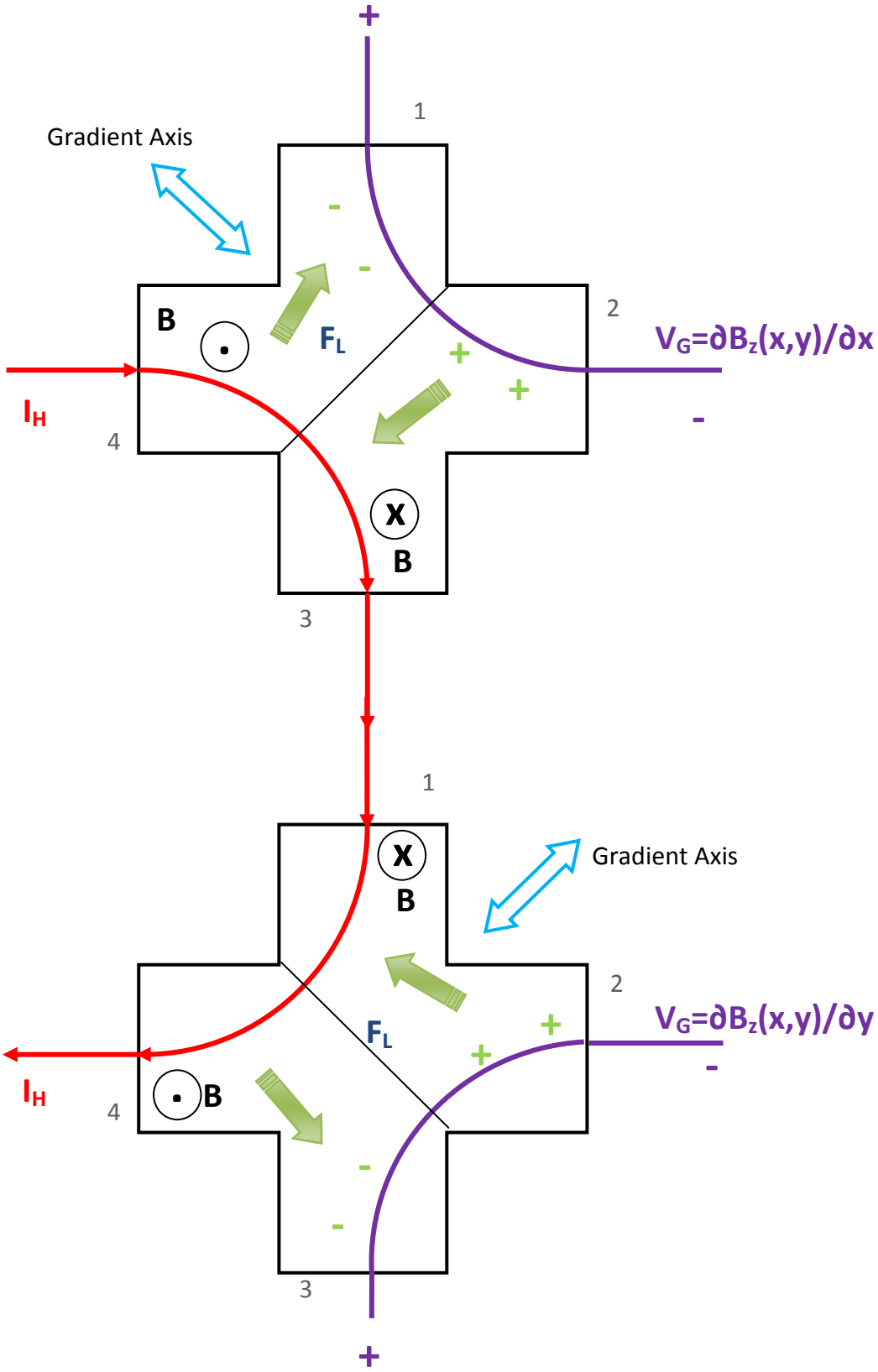

Figure 3: Hall effect with non-perpendicular current and voltage leads with different configurations under non-uniform magnetic field.

The scan performed with a speed of 5µm/s at 256 pixel resolution, applying a 500µA DC drive current to the probe in the AFM tracking mode. Figure 5 shows the SHPM image of the Hard Disk sample resolving individual bits. The Hall sensor alignment and the lead configurations are given at the right hand side of the figure.

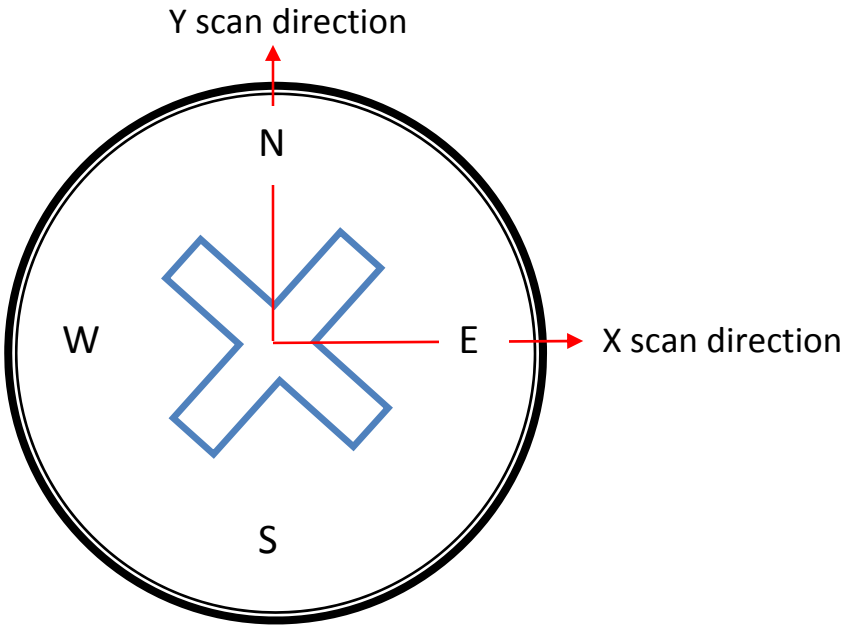

Figure 4: Orientation of the Hall sensor, over the sample, with respect to the scan direction of the microscope: Hall cross has 45° alignment.

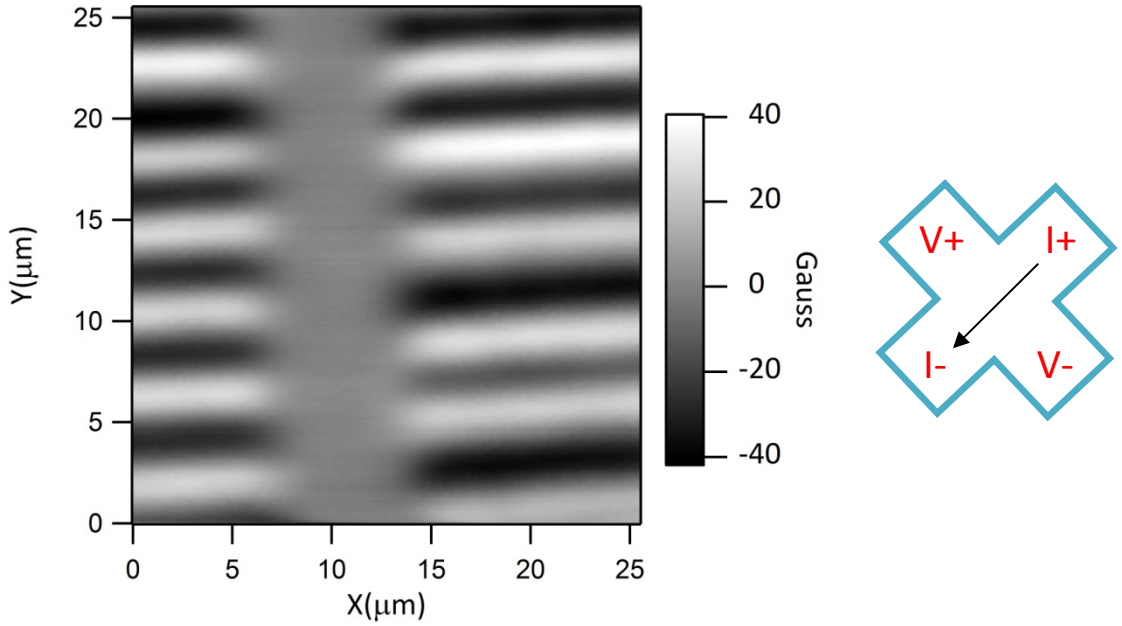

Figure 5: SHPM scan of a Hard disk sample at 77K with normal Hall sensor configuration of mutually perpendicular current and voltage leads. Hall cross diagram shows the relative alignment of the probe over the sample and the leads' positions.

The magnitude of the Hall voltage signal is stored in a 256×256 matrix. Hence, matrix arithmetic operations can be applied on the acquired image. Equipped with these, the rows are differentiated along the *y* direction to obtain $\partial \mathbf{B_z}/\partial \mathbf{x}$, and columns are differentiated to get $\partial \mathbf{B_z}/\partial \mathbf{y}$ along the *x* direction using forward differences method. The results are shown in Fig 6 and Fig 7 which are calculated $\partial \mathbf{B_z}/\partial \mathbf{x}$ and $\partial \mathbf{B_z}/\partial \mathbf{y}$ respectively. Immediately after obtaining the standard SHPM image, drive current direction is changed to the proper leads so that the $\partial \mathbf{B_z}/\partial \mathbf{x}$ and $\partial \mathbf{B_z}/\partial \mathbf{y}$ images can be obtained. To have a healthy comparison, the probe was not pulled back off the surface while the switch positions on the amplifier are changed. The Hall probe was driven by smaller, 100µA current, as it was not possible to properly offset null the probe. The other scan parameters are held the same as in the case of normal scan. Images obtained as a result of these experiments and the current/ voltage lead configurations are shown in Fig. 8 and 9. The results are in perfect agreement with the calculated ones, except the field values are not absolute since the probe is offset nulled at the presence of the field.

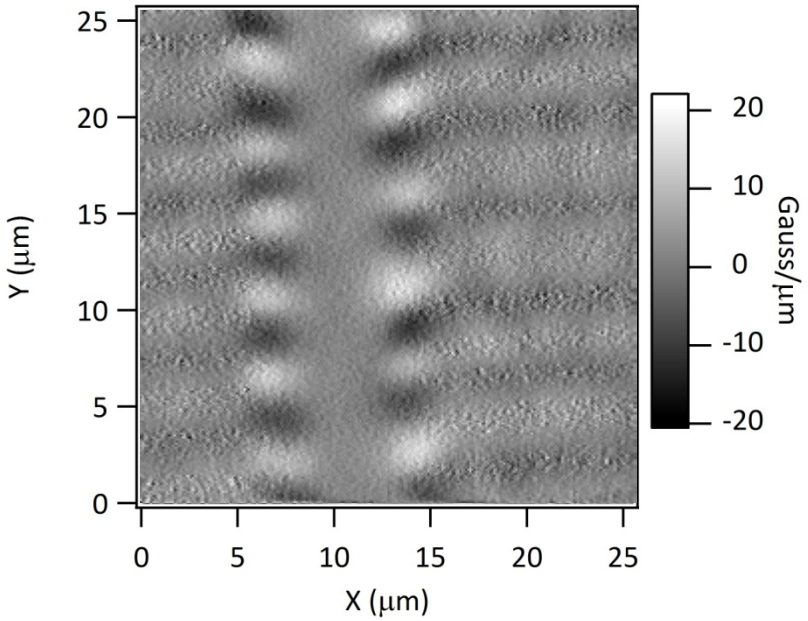

Figure 6: Calculated $\partial B_z/\partial x$ *from the measured* $B_z(x,y)$ *data matrix by forward differences.*

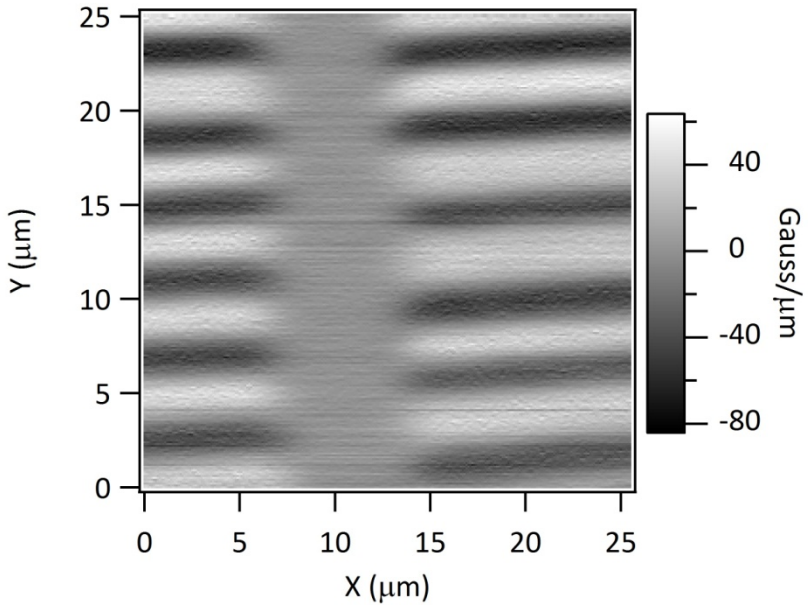

Figure 7: Calculated $\partial B_z/\partial y$ *from the measured* $B_z(x,y)$ *data matrix by forward differences.*

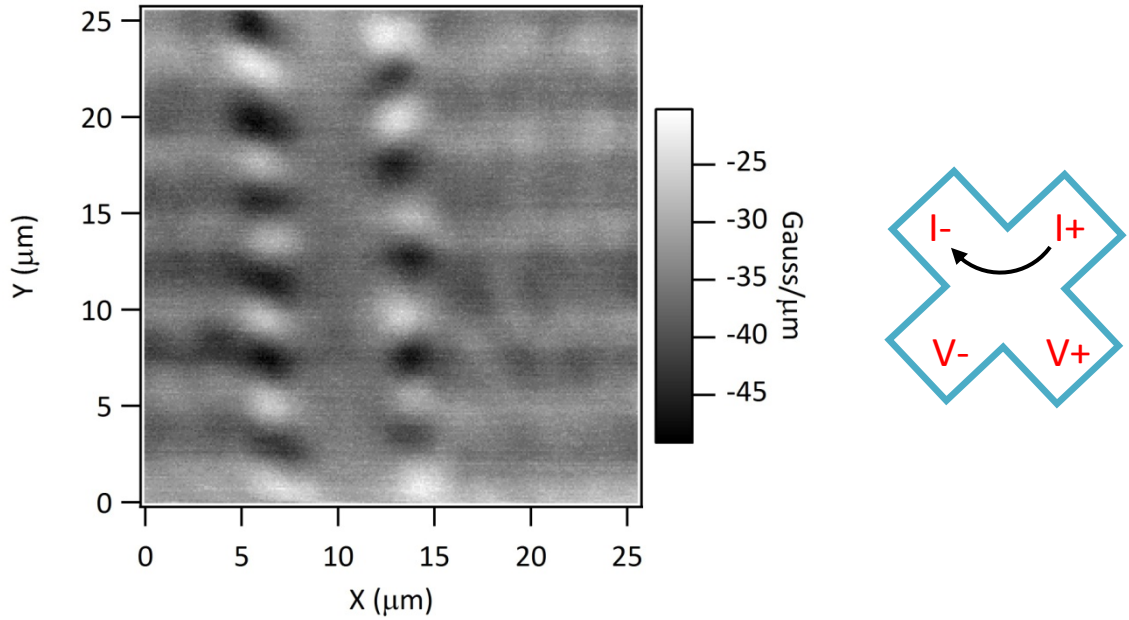

Figure 8: SHPM scan of a HDD at 77K with Hall sensor configuration shown in the diagram. The image represents $\partial B_z/\partial x$ *due to the relative positions of current and voltage leads*

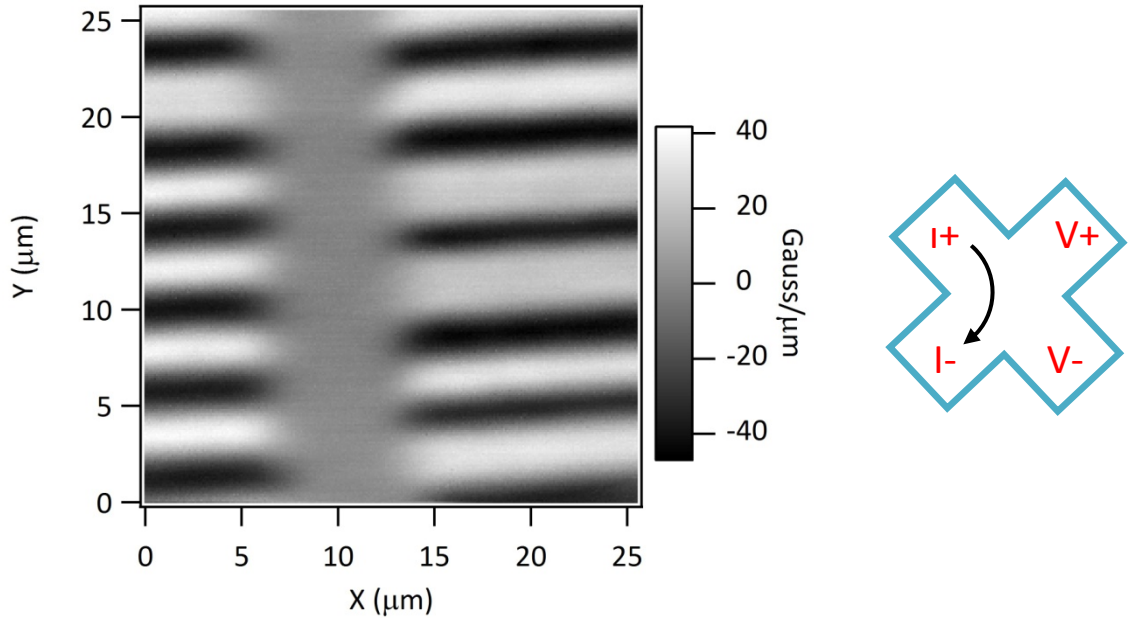

Figure 9: SHPM scan of a HDD at 77K with Hall sensor configuration shown in the diagram. The image represents $\partial B_z/\partial y$ *due to the relative positions of current and voltage leads.*

1.2 Three Dimensional Magnetic Field Imaging

As different sample orientations are scanned, different images are obtained in lateral derivative, which was actually expected as the gradient of the field changes in the space. One may argue that since we can calculate the local gradient of the $\mathbf{B_z(x,y)}$ along ***x*** and ***y*** directions, why should we bother imaging in this obscure way? On the other hand this measurement mode clearly gives us the local gradient of the $\mathbf{B_z(x,y)}$, which can be used in a number of applications like gradiometry etc.

A more important ramification is the possibility of calculating in-plane components, $\mathbf{B_x(x,y)}$ and $\mathbf{B_y(x,y)}$ of the magnetic field if we *measure* $\mathbf{B_z(x,y)}$, $\partial\mathbf{B_z(x,y)}/\partial\mathbf{x}$ and $\partial\mathbf{B_z(x,y)}/\partial\mathbf{y}$ across the space. If we start with the Maxwell equation derived from Ampere's law [5],

$$\vec{\nabla} \times \vec{B} = \varepsilon_0 \mu_0 \vec{J} + \varepsilon_0 \mu_0 \frac{\partial \vec{E}}{\partial t} \tag{1}$$

In a source free region the equation simplifies to,

$$\vec{\nabla} \times \vec{B} = 0 \tag{2}$$

which can be written, in open form, as

$$\left(\frac{\partial}{\partial x}\hat{\imath} + \frac{\partial}{\partial y}\hat{\jmath} + \frac{\partial}{\partial z}\hat{k}\right) \times \left(B_x\hat{\imath} + B_y\hat{\jmath} + B_z\hat{k}\right) = 0 \tag{3}$$

from which we can get,

$$\left(\frac{\partial B_z}{\partial y} - \frac{\partial B_y}{\partial z}\right)\hat{\imath} - \left(\frac{\partial B_z}{\partial x} - \frac{\partial B_x}{\partial z}\right)\hat{\jmath} + \left(\frac{\partial B_y}{\partial x} - \frac{\partial B_x}{\partial y}\right)\hat{k} = 0 \tag{4}$$

To satisfy the equation each vector component must individually be equal to zero.

$$\left(\frac{\partial B_z}{\partial y} - \frac{\partial B_y}{\partial z}\right) = 0 \tag{5}$$

$$\left(\frac{\partial B_z}{\partial x} - \frac{\partial B_x}{\partial z}\right) = 0 \tag{6}$$

$$\left(\frac{\partial B_y}{\partial x} - \frac{\partial B_x}{\partial y}\right) = 0 \tag{7}$$

The first two equations can be solved in terms of the parameters we measure at the beginning of the problem. Hence we can write,

$$\left(\frac{\partial B_z}{\partial y} - \frac{\partial B_y}{\partial z}\right) = 0 \tag{8}$$

$$\Rightarrow \frac{\partial B_z}{\partial y} = \frac{\partial B_y}{\partial z} \tag{9}$$

$$B_y = \int_z^{\infty} \frac{\partial B_z}{\partial y}\, dz \tag{10}$$

Hence if we measure or obtain $\partial \mathbf{Bz}/\partial \mathbf{y}$ as a function of z, then we can calculate the $\mathbf{B_y}$ at this specific z. The SHPM data should be obtained at increasing sample-sensor distances, until the signal decays to zero or below the noise levels. A similar equation can be written for $\mathbf{B_x}$ as well,

$$B_x(x, y, z) = \int_z^{\infty} \frac{\partial B_z(x,y,z')}{\partial x}\, dz' \tag{11}$$

As, it is not possible to integrate the equations analytically, we have to compute them numerically from the measured data.

$$\int_z^{\infty} f(z')\, dz' \cong h\left[\sum_{j=1}^{n} f(jh)\right] \tag{12}$$

The situation can visualized with the aid of Fig. 10 given below. While we can measure the quantitative value of the perpendicular magnetic field, $\mathbf{B_z}$, at the closest sample-sensor position, this is not exactly the case for the derivatives. The change in magnitude at a particular point for, $\partial \mathbf{B_z(x,y,z)}/\partial \mathbf{x}$ and $\partial \mathbf{B_z(x,y,z)}/\partial \mathbf{y}$ is not necessarily a decrease with increasing sample-sensor separation. However, the overall dynamic field will decrease with increasing probe-sample separation.

Note that we do not need to have an infinite sum as the field value *f(jh)* will decay after a certain value of *jh* that can be set as the finite upper limit *n*. Thus, $\partial \mathbf{B_z(x,y,z)}/\partial \mathbf{x}$ and $\partial \mathbf{B_z(x,y,z)}/\partial \mathbf{y}$ are acquired at different heights (z_i) until the field decays to zero, carefully recording the values. A fixed incremental separation $\boldsymbol{h}$ is used between the scans for ease of calculation.

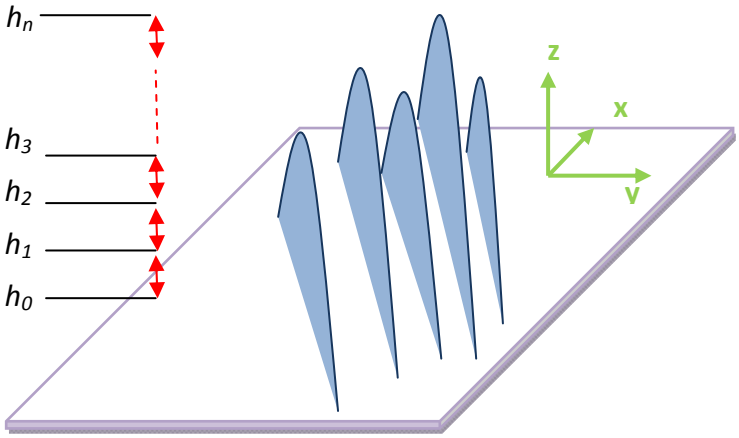

Figure 10: Visualization of incremental scan for $B_z(x,y,z)$, $\partial B_z(x,y,z)/\partial x$ and $\partial B_z(x,y,z)/\partial y$

While the sample is scanned the surface is never perfectly smooth. In addition to this, some inclination angle can unintentionally be given, while mounting the sample. For this reason, while the sample is scanned with a liftoff, this distance must be applied throughout the sample evenly. The magnetic force microscopy (MFM) techniques, where the magnetic and interaction forces have to be separated, can be applied to this

case. Hence, while the forward scan is conducted using the feedback following the surface texture; the backward scan is performed following the same texture, however this time, by adding the required lift-off value at each pixels. By this procedure, the value of $\boldsymbol{h}$ is held fixed throughout the whole scan area. Fig 11 shows the image of Hard disk with the forward scan, (a) while the probe is in closest proximity of the sample, and backward scan (b) while the probe is lifted off by 3.5µm. The decay of the magnetic signal when the probe is lifted off by 3.5µm away from the surface can clearly be seen and obviously this distance can be accepted as the upper limit of the integration while calculating the $\mathbf{B_x}$ and $\mathbf{B_y}$. This value is within the range of retraction capability of the used scanner piezo at room temperature. But, unfortunately, the effect of the thermal drift is also high at room temperature and it is virtually impossible to scan the same portion of the HDD by giving successive offsets, which is required to integrate $\boldsymbol{\partial B_z/\partial x}$ or $\boldsymbol{\partial B_z/\partial y}$. Fig 12 shows this effect. At each level of 0.5µm offset, three images, B_z, $\partial B_z/\partial x$ and $\partial B_z/\partial y$, had to be recorded. Each image requires ~40 minutes to be scanned. Hence, approximately two hours spent at each level. As a result, the experiments had to be done at low temperature to eliminate the thermal drift, which unfortunately reduces the scan area of the piezo tube in X, Y and Z directions. To satisfy both requirements, the stick-slip coarse approach mechanism is used to successively pull the Hall sensor off the sample. The motion of the puck is first calibrated for a given voltage pulse. Then appropriate numbers of pulses were applied in order to lift-off the sensor from the sample. We adjusted the voltage pulses applied to the piezo to provide 250nm backward steps. Overall 26 scans are performed, starting from the closest proximity of the sample, with 250nm steps, until the probe is 6.5µm away from the sample in height. At each height level, $\mathbf{B_z}\boldsymbol{(x,y)}$, $\boldsymbol{\partial B_z(x,y)/\partial x}$ and $\boldsymbol{\partial B_z(x,y)/\partial y}$ were imaged. The thermal drift is insignificant at 77K as evident in Fig 13. $\boldsymbol{\partial B_z/\partial x}$ and $\boldsymbol{\partial B_z/\partial y}$ images are used to integrate $\mathbf{B_x}$ and $\mathbf{B_y}$ respectively using the method described above. Figures 14-16 show the $\mathbf{B_z}$, $\mathbf{B_y}$ and $\mathbf{B_x}$ fields of an Hard disk sample.

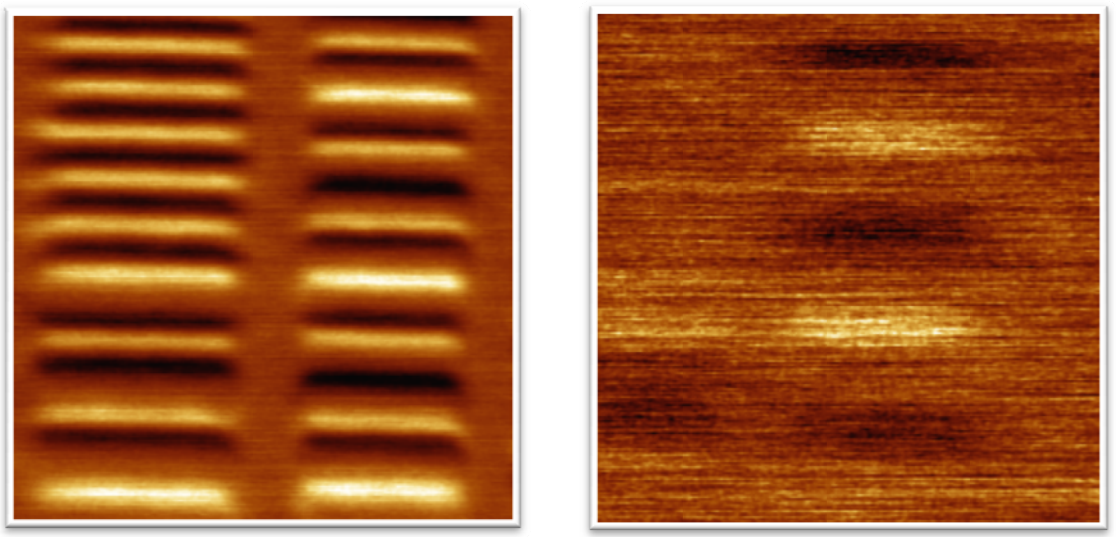

(a) (b)

Figure 11: SHPM image of Hard disk sample, (a) forward scan (in the tunneling range) and (b) backward scan (3.5µm away from the surface). Both images were obtained with STM feedback. Scan speed was 5µm/s, resolution set to 256 × 256 pixels, -100mV bias voltage applied to the sample and the tunneling current of 1nA maintained during the scan.

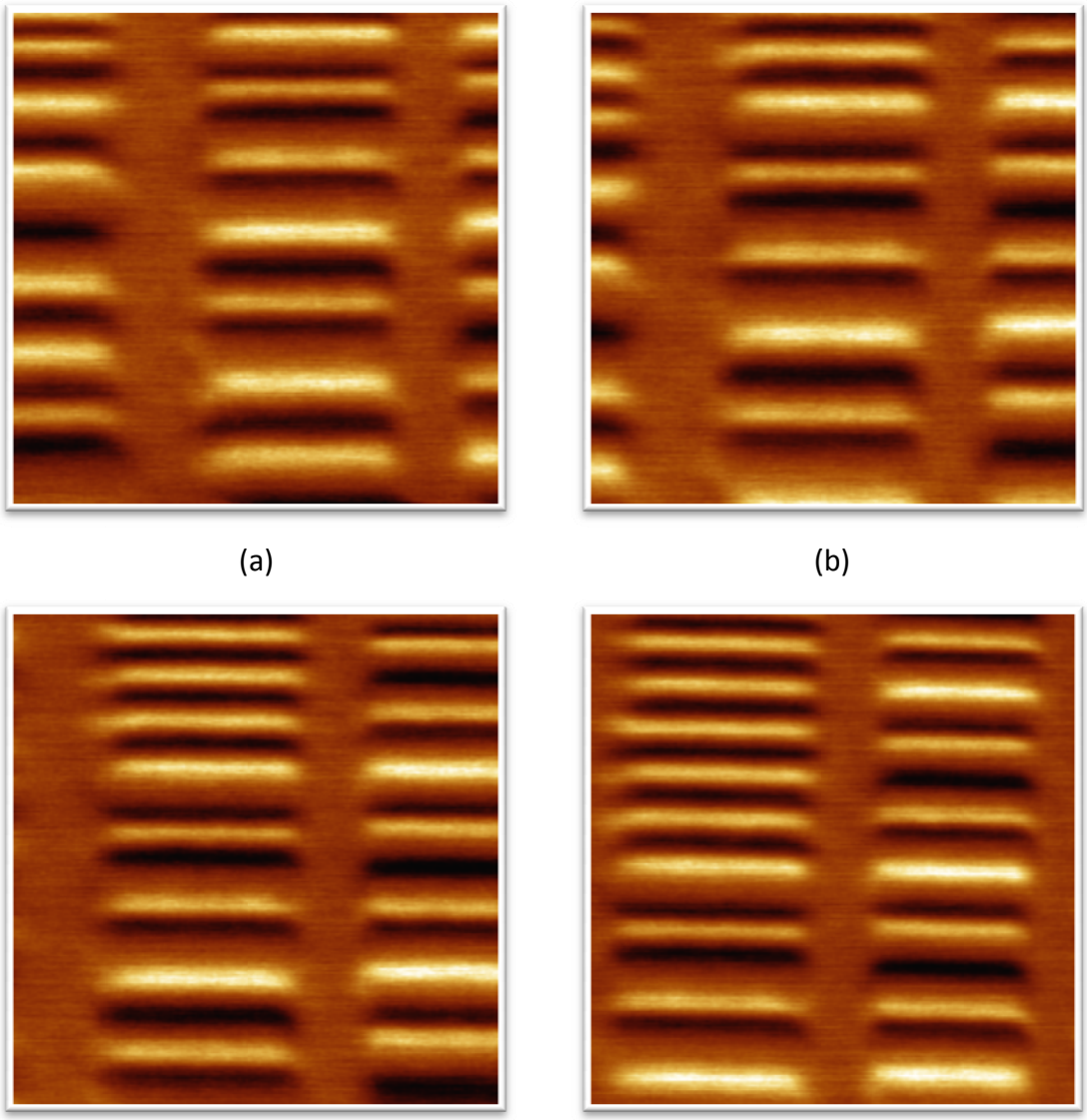

Figure 12: SHPM images of Hard disk sample obtained at room temperature showing effect of the thermal drift. Pictures are the forward scans of probe above the sample with a height of (a) 0.5µm, (b) 1.5µm, (c) 2.5µm, (d) 3.5µm respectively. Field decay is not seen as the offset is only given during the backward scan. Approximately 4 hours of time passed between the shown images. The shift is towards the bottom left corner. All images were obtained with STM feedback using a 1µm PHEMT sensor. Scan speed was 5µm/s, resolution set to 256 × 256 pixels, -100mV bias voltage applied to the sample and the tunneling current of 1nA maintained during the scan.

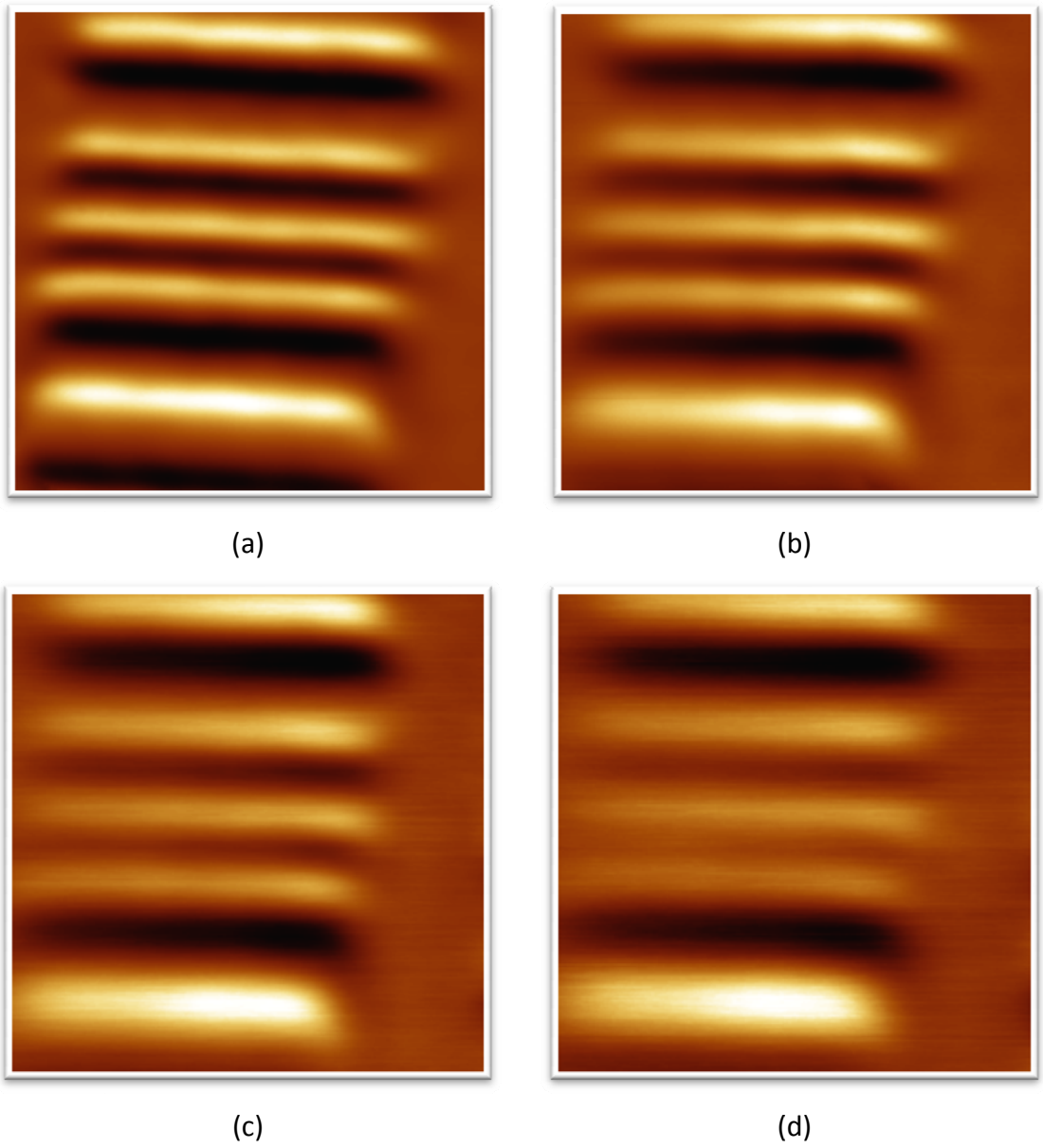

Figure 13: SHPM images of Hard disk sample obtained at 77K showing effect of the thermal drift. Pictures are the scans of probe levels above the sample with a height of (a) 0.25 µm, (b) 1.25µm, (c) 2.5µm, (d) 3.75µm respectively. Approximately 10 hours passed between the first and the last images. There is a very little drift which becomes insignificant after thermal stabilization. All images were obtained using a 1µm PHEMT sensor. Scan speed was 5µm/s, resolution set to 256 × 256 pixels. The decay of the magnetic field can also be seen as the sensors moves away from the sample.

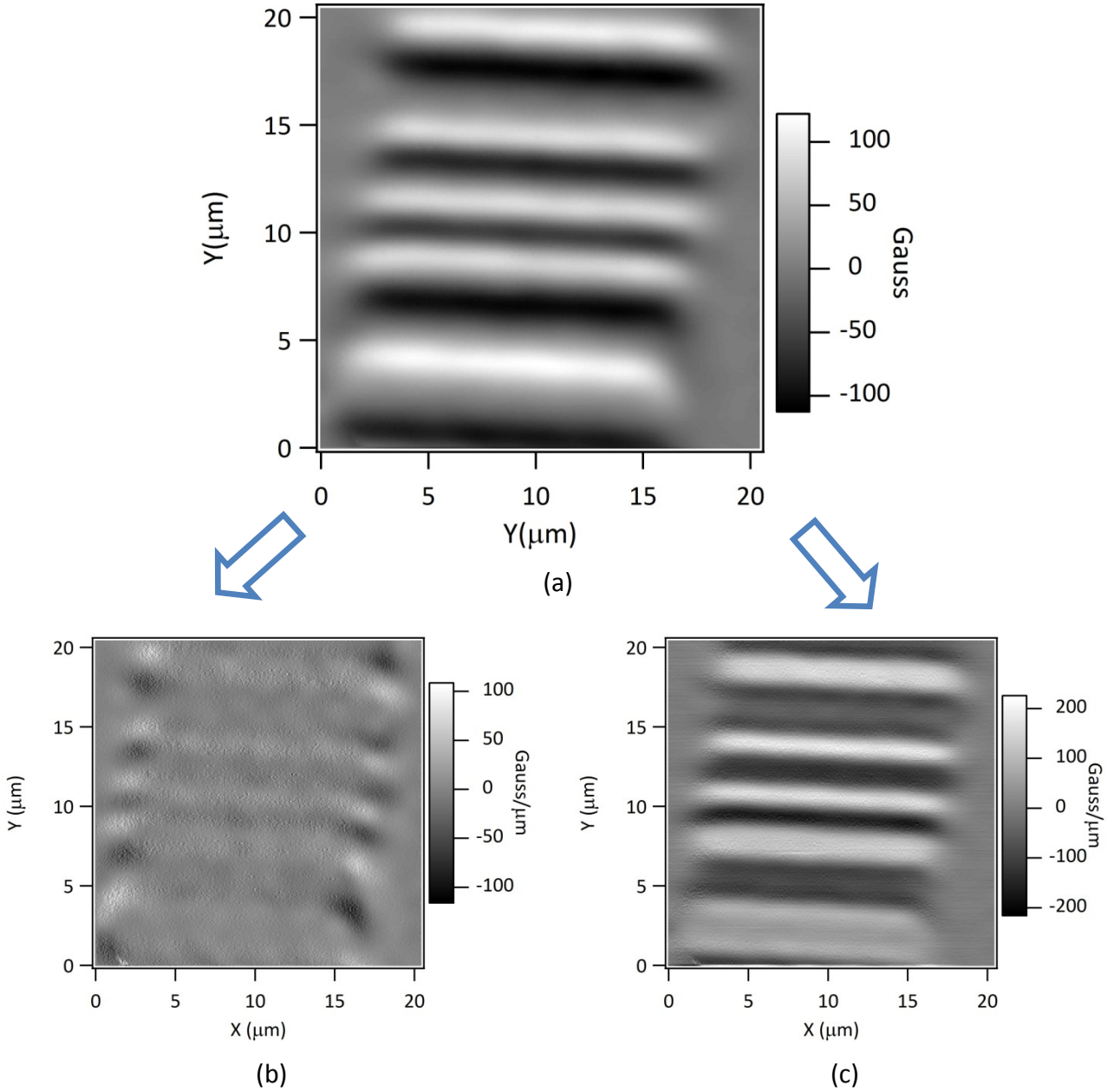

Figure 14: SHPM image of Hard disk sample, shows the $\boldsymbol{B_z}$ *of the field (a), obtained at 77K in the feedback tracking zone. Image was obtained using a 1µm PHEMT sensor. Scan speed was 5µm/s, resolution set to 256×256 pixels.* $\boldsymbol{\partial B_z(x,y)/\partial x}$ *(b) and* $\boldsymbol{\partial B_z(x,y)/\partial y}$ *(c) are calculated from* $\boldsymbol{B_z}$ *image by differentiating rows and columns of the image matrix respectively.*

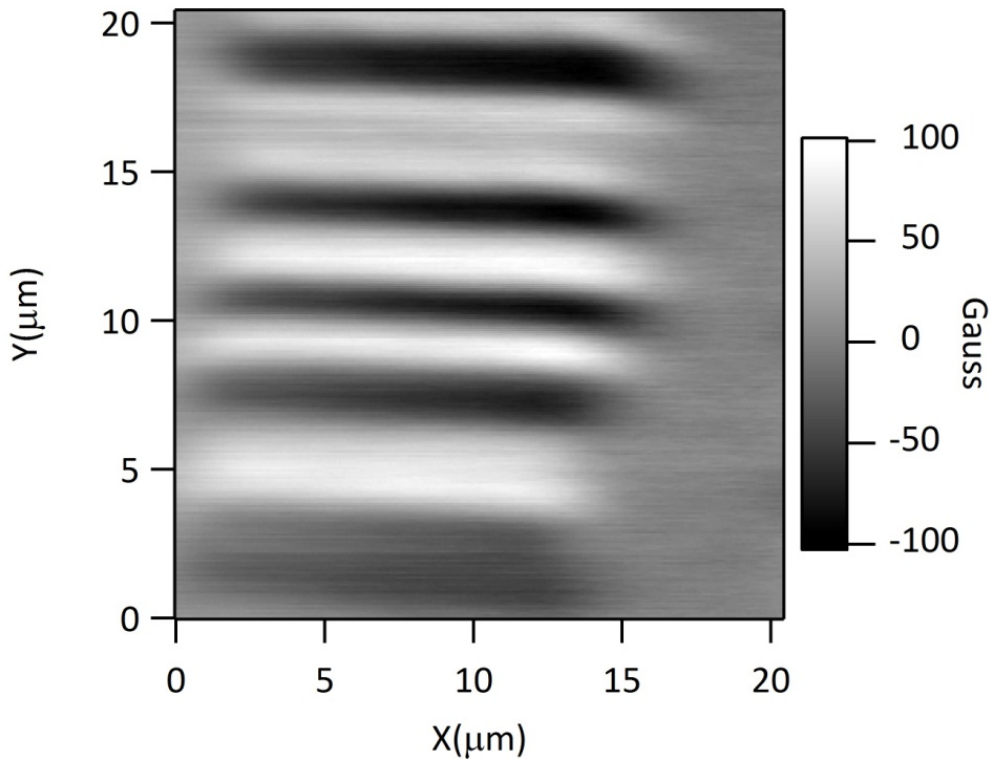

*Figure 15: $\boldsymbol{B_y}$ field calculated by integrating $\boldsymbol{\partial B_z/\partial y}$ over a finite range. Each image file used in calculation was obtained using the same 1µm PHEMT sensor. Scan speed was 5µm/s, resolution set to 256×256 pixels. The increments along the z-direction, **h**, is set to 0.25µm in the range of [0, 6.5µm].*

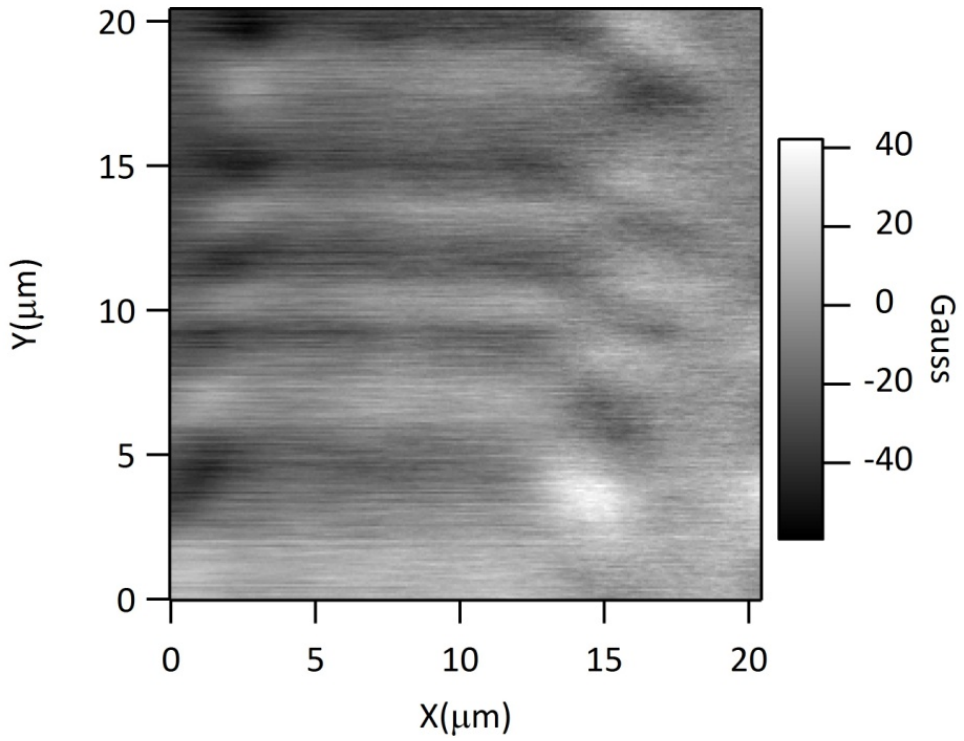

*Figure 16: $\boldsymbol{B_x}$ field calculated by integrating $\boldsymbol{\partial B_z/\partial x}$ over a finite range. Each image file used in calculation was obtained using the same 1µm PHEMT sensor. Scan speed was 5µm/s, resolution set to 256×256 pixels. The increments along the z-direction, **h**, is set to 0.25µm in the range of [0, 6.5µm].*

1. Sandhu, A., et al., *50 nm Hall sensors for room temperature scanning Hall probe microscopy.* Japanese Journal of Applied Physics Part 1-Regular Papers Short Notes & Review Papers, 2004. **43**(2): p. 777-778.
2. Grundler, D., et al., *Bend-resistance nanomagnetometry: spatially resolved magnetization studies in a ferromagnet/semiconductor hybrid structure.* Physica E-Low-Dimensional Systems & Nanostructures, 2002. **12**(1-4): p. 248-251.
3. Peeters, F.M. and X.Q. Li, *Hall magnetometer in the ballistic regime.* Applied Physics Letters, 1998. **72**(5): p. 572-574.
4. Oral, A., unpublished.
5. Jackson, J.D., *Classical Electrodynamics*. 3rd ed. 1999, New York: Wiley. xxi, 808 p.